NUCL SCI TECH (2018) 29:115
https://doi.org/10.1007/s41365-018-0444-7

Upgrade of the X-ray pinhole camera system at SSRF

Bo Gao[1,2] · Yong-Bin Leng[1,2] · Han-Jiao Chen[1,2] · Jie Chen[1] · Kai-Rong Ye[1]

Received: 9 January 2018 / Revised: 10 April 2018 / Accepted: 11 April 2018 / Published online: 4 July 2018

Abstract An X-ray pinhole camera has been used to determine the transverse beam size and emittance on the diagnostic beam line of the storage ring at SSRF since 2009. The performance of the beam size measurement is determined by the width of the point spread function of the X-ray pinhole camera. Beam-based calibration was carried in 2012 out by varying the beam size at the source point and measuring the image size. However, this calibration method requires special beam conditions. In order to overcome this limitation, the pinhole camera was upgraded and an X-ray quasi-monochromator was installed. A novel experimental method was introduced by combining the pinhole camera with the monochromator to calibrate the point spread function. The point spread function can be accurately resolved by adjusting the angle of the monochromator and measuring the image size. The X-ray spectrum can also be obtained. In this work, the X-ray quasi-monochromator and the novel beam-based calibration method will be presented in detail.

Keywords X-ray pinhole camera · Transverse beam size · Diagnostic beam line · Point spread function · X-ray quasi-monochromator

This work was supported by the National Science Foundation of China (No.11375255).

✉ Yong-Bin Leng
lengyongbin@sinap.ac.cn

1 Shanghai Institute of Applied Physics, Chinese Academy of Sciences, Shanghai 201800, China

2 University of Chinese Academy of Sciences, Beijing 100049, China

1 Introduction

The Shanghai Synchrotron Radiation Facility (SSRF) is a third-generation synchrotron light source with the primary goal of generating low emittance light. The emittance is 3.9 nm.rad in the SSRF storage ring, the variation in the transverse beam size at the source point of the X-ray diagnostic beam line is σ_x 73 μm and σ_y 22 μm in the horizontal and vertical directions, respectively. X-ray pinhole cameras are widely used to measure the transverse beam size and emittance at many facilities [1–4]. An X-ray pinhole camera system has been installed on the diagnostic beam line, and the basic layout and components of this system are shown in Fig. 1 [5, 6].

For the X-ray pinhole camera, the real beam size is a function of the image size and the point spread function (PSF) of the system. The performance of the pinhole camera is quantified using the width of the PSF. The main contributors to the PSF width are the PSF of the pinhole and the PSF of the imaging system. Assuming that the PSF is Gaussian, these two contributions add quadratically to the complete PSF.

In order to determine the practical value of the PSF, an online experiment was introduced in 2012 [7]. The practical value of the PSF can be derived by varying the beam size at the source point and measuring the image size. A more accurate system resolution can be measured from this calibration procedure. However, this experimental method requires special beam conditions that cannot be carried out in the user operation mode.

To overcome the limitation of the previous calibration method, a novel beam-based experimental method was introduced. Because synchrotron radiation extracted from the bending magnet is emitted with a wide range of

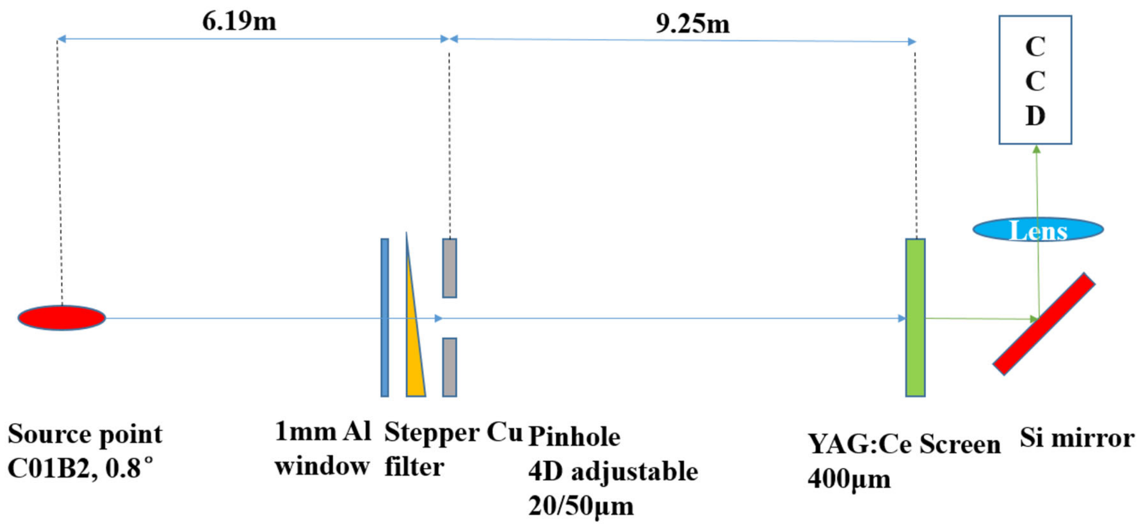

Fig. 1 (Color online) System layout of the SSRF X-ray pinhole camera

energies, the PSF from different wavelengths cannot be ignored. If the wavelength of the extracted X-ray changes, the contribution from diffraction and the images will be changed. A new calibration method was developed based on these considerations. The PSF is expected to be calibrated by selecting X-rays with different wavelengths and recording the change in the imaging spot size. The monochromatic crystal is a good tool for selecting a defined X-ray wavelength. Therefore, an X-ray quasi-monochromator was installed. Combined with this monochromator, the new pinhole system is expected to enable calibration of the PSF under any beam conditions. Technical details and experiments will be discussed in this paper.

Setup of the X-ray quasi-monochromator and a PSF study of the new pinhole camera are presented in detail in the following section. Beam experiments are presented in Sect. 3. Next, an application of the new pinhole camera is presented. Finally, a novel experimental method for calibrating the PSF is presented in the final section.

2 X-ray quasi-monochromator of pinhole camera at SSRF

X-ray monochromators are widely used in X-ray-focused imaging systems in many diagnostic beam lines [8, 9]. In this work, the X-ray quasi-monochromator was used to calibrate the PSF of a pinhole camera.

2.1 Principles of X-ray quasi-monochromators

X-ray monochromators are analogous to grating monochromators and spectrometers in the visible spectrum [10]. If the lattice spacing for a crystal is accurately known, the observed angles of diffraction can be used to measure and identify unknown X-ray wavelengths. Because of the sensitive wavelength dependence of Bragg reflection exhibited by materials like silicon, a small portion of a continuous spectrum of radiation can be isolated [10]. Bent single crystals used in X-ray spectroscopy are analogous to the curved line gratings used in optical spectroscopy. After the beam has passed through a high-resolution monochromator, the spectral bandwidth can be as narrow as 10^{-4} [10]. A crystal monochromator operates through the diffraction process according to Bragg's law. Photon energy (wavelength) can be selected by crystal, net planes, and Bragg angle.

The Bragg's law is presented in Eq. (1):

$$2d\sin\theta = n\lambda, \tag{1}$$

where d is the lattice spacing of the crystal, θ is the glancing angle, and n is the diffraction order. The lattice spacing is 0.314 nm in the case of an Si(111) crystal. The energy of the diffracted X-rays is determined by the glancing angle θ, which is shown in Fig. 2. For Bragg angles ranging from 3° to 70°, the detected energy range is between 2 and 40 keV. Energy resolution is a very important parameter for a monochromator system. An Si(111) crystal has an energy resolution ranging from 10^{-5} to 10^{-3}.

2.2 Setup of the X-ray quasi-monochromator

According to the X-ray monochromator principles presented in the previous section, it can be seen that a typical X-ray monochromator generally consists of a silicon crystal and an accurate rotating rail stack.

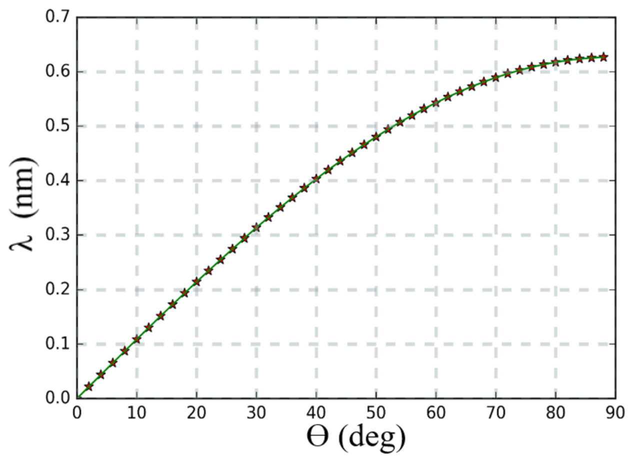

Fig. 2 (Color online) Energy and wavelength as a function of glancing angle θ

The selected crystal should be able to cover the main spectral range for synchronous light. Spectra of the extracted X-rays are shown in Fig. 8. The properties and performance of Si(111) crystals are described in the previous section, and Si(111) crystal is able to meet the requirements of this work. In order to realize the selection of different wavelengths, the SGSP-60YAW rotating rail from SIGMAKOKI [11] was selected, which has a rotating accuracy of 0.005 deg/pulse. Figure 3 shows the schematic of the X-ray quasi-monochromator for the X-ray pinhole camera. This quasi-monochromator is mounted on a rail that can be moved in and out of the optical path of the X-ray pinhole camera.

Fig. 3 (Color online) X-ray quasi-monochromator for X-ray pinhole camera at SSRF

The former X-ray pinhole camera system is shown in Fig 1. The addition of a single crystal to the light path requires consideration of the position of the existing YAG:Ce target or the position of the camera. Because of the glancing angle, the reflected X-ray will deviate from the original imaging point. In order to keep the X-ray within the range of the YAG:Ce scintillator screen, the monochromator crystal was placed close to the imaging system. The relationship between the distance from the monochromatic crystal to the YAG:Ce target and the deviation of the reflected light from the YAG:Ce center are shown in Fig. 4. In this case, the distance between the center of the crystal and the YAG:Ce target is 8 cm. The layout of the new X-ray pinhole camera is shown in Fig. 5.

A study on the PSF of the new X-ray pinhole camera is presented in the next subsection.

2.3 Point spread function study of the new X-ray pinhole camera

The image formed on the camera is the convolution of several independent contributions, including the beam size, pinhole, and the imaging system. We assume the source and the PSFs to be Gaussian. The root mean square (RMS) beam size can be expressed as follows [12]:

$$\sigma_{\mathrm{beam}} * C_{\mathrm{mag}} = \sqrt{\sigma_{\mathrm{img}}{}^2 - \sigma_{\mathrm{aper}}{}^2 - \sigma_{\mathrm{diff}}{}^2 - \sigma_{\mathrm{scr}}{}^2}, \tag{2}$$

where C_{mag} is the magnification factor of the X-ray pinhole system, σ_{img} is the acquired image size, σ_{aper} is the geometric width of the pinhole PSFs, σ_{diff} is the diffraction width, and σ_{scr} is the imaging system width, which contains the effects of the YAG:Ce scintillator screen, lens, and CCD camera.

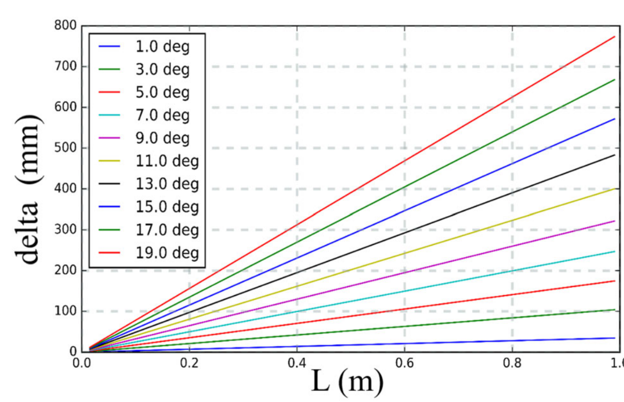

Fig. 4 (Color online) Distance between the monochromatic crystal 'L' and the YAG:Ce target and the deviation of the reflected light from the YAG:Ce center 'delta'

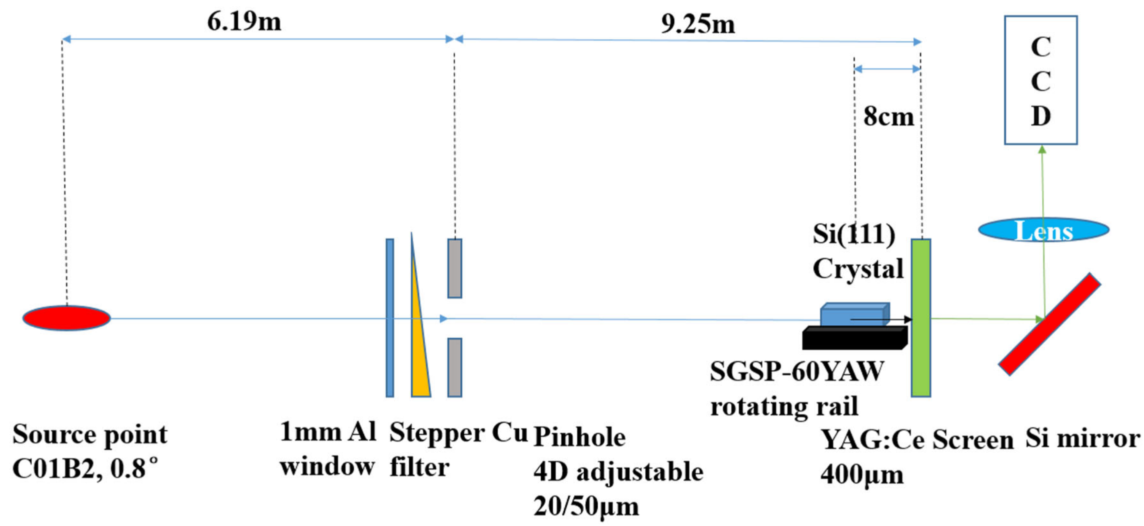

Fig. 5 (Color online) Schematic of the X-ray pinhole camera combined with a quasi-monochromator

The diffraction width of the pinhole PSFs for a monochromatic photon beam is given by [12]

$$\sigma_{\mathrm{diff}} = \frac{\sqrt{12}\lambda D}{4\pi A}, \tag{3}$$

where A is the aperture size of the pinhole, D is the distance from the pinhole to the YAG:Ce target, and λ is the wavelength of the X-ray. The difficulty in this experiment involves determining the wavelength. For the former system, the method integrates this expression over the spectrum [7]. For the new pinhole camera, the wavelength can be calculated from the glancing angle. However, it is very hard to measure this angle directly. Therefore, a beam-based experimental method was employed to measure the glancing angle, which will be presented in the next section.

The geometric width of pinhole PSFs is given by [12]

$$\sigma_{\mathrm{aper}} = \frac{A(D+d)}{\sqrt{12}d}, \tag{4}$$

where d is the distance from the source point to the pinhole.

However, the PSF of the imaging system is hard to calculate. The imaging system is shown in Fig. 5. The CCD camera used in this work is Point Grey FL2-08S2M, which has a 12-bit ADC and has a resolution of 1031 × 776 pixels at 30 FPS with 4.65 μm/pixel. Introducing a lens doubles the magnification of the imaging system . An experiment has been conducted at SSRF to measure the PSF of the imaging system [13].

3 Beam experiments

Several experiments are presented in this section. The first experiment is used to verify that the obtained X-ray is quasi-monochromatic, which is the basis of all further experiments. Then the measurement of the wavelength is described, which is required for accurate calibration of the PSF. Next, the beam-based calibration method is presented. The section concludes with a discussion of the results.

3.1 Verifying the presence of quasi-monochromatic X-ray

The monochromator is based on Bragg reflection, and monochromatic light is reflected from the crystal surface. If the light that reaches the target is reflected light, and the spot position moves with the crystal. In addition, the monochromatic beam energy will also be lower than the energy of the full synchrotron spectrum. The idea of this experiment is to move the crystal and observe the resulting images.

Since the crystal surface was perpendicular to the YAG:Ce scintillator screen. In order to conveniently observe the reflected light on the CCD, the crystal was rotated 0.5 degrees before the experiment. Then the crystal was moved slowly into the light path. The process of verification is shown below.

First, the entire image of the photon at the source point was found at the CCD camera. When the edge of the spot in the observed image was obscured, it seems that the edge of the crystal begins obstructing the light path. Next, the crystal was moved further into the beam, and the spot on the CCD camera was also moved, resulting in an intensity decrease. This experiment was carried out using 500 electron beam bunches in the storage ring, and the current was approximately 200 mA. A 2 mm Cu filter was inserted in the light path, and the size of the rectangle pinhole was $50\,\mu m \times 20\,\mu m$. The exposure time of the CCD was 0.01 s, and the gain was 16 dB. Images in this process are shown in Fig. 6.

Figure 6 shows three typical results of the experiment presented above, and the profile was obtained using direct projection. Those figures show that during the last step of the experiment presented above, the intensity decreased as the spot moved. According to the verification ideas described above, the last image shows how X-rays are reflected from the crystal. In other words, this can be considered as quasi-monochromatic X-ray imaging. However, the intensity was very low, the Cu filter was been moved out before the next experiment. The image obtained at the camera can be seen in Fig. 7.

The images show horizontal compression due to the inherent deformation of the crystal surface in the horizontal direction and the angle of the YAG:Ce scintillator screen. This paper focuses on the vertical direction, and the vertical beam size measurement will be presented in the following sections.

3.2 Measurement of wavelength

After verifying that the X-ray is monochromatic, the next important thing is to determine the X-ray wavelength, which is very important for calculating the diffraction width of PSFs.

A spectrum is a very useful tool that can be used to characterize the intensity distribution at each wavelength of synchrotron light. If the intensity of the X-rays at each wavelength can be measured, the spectrogram can be

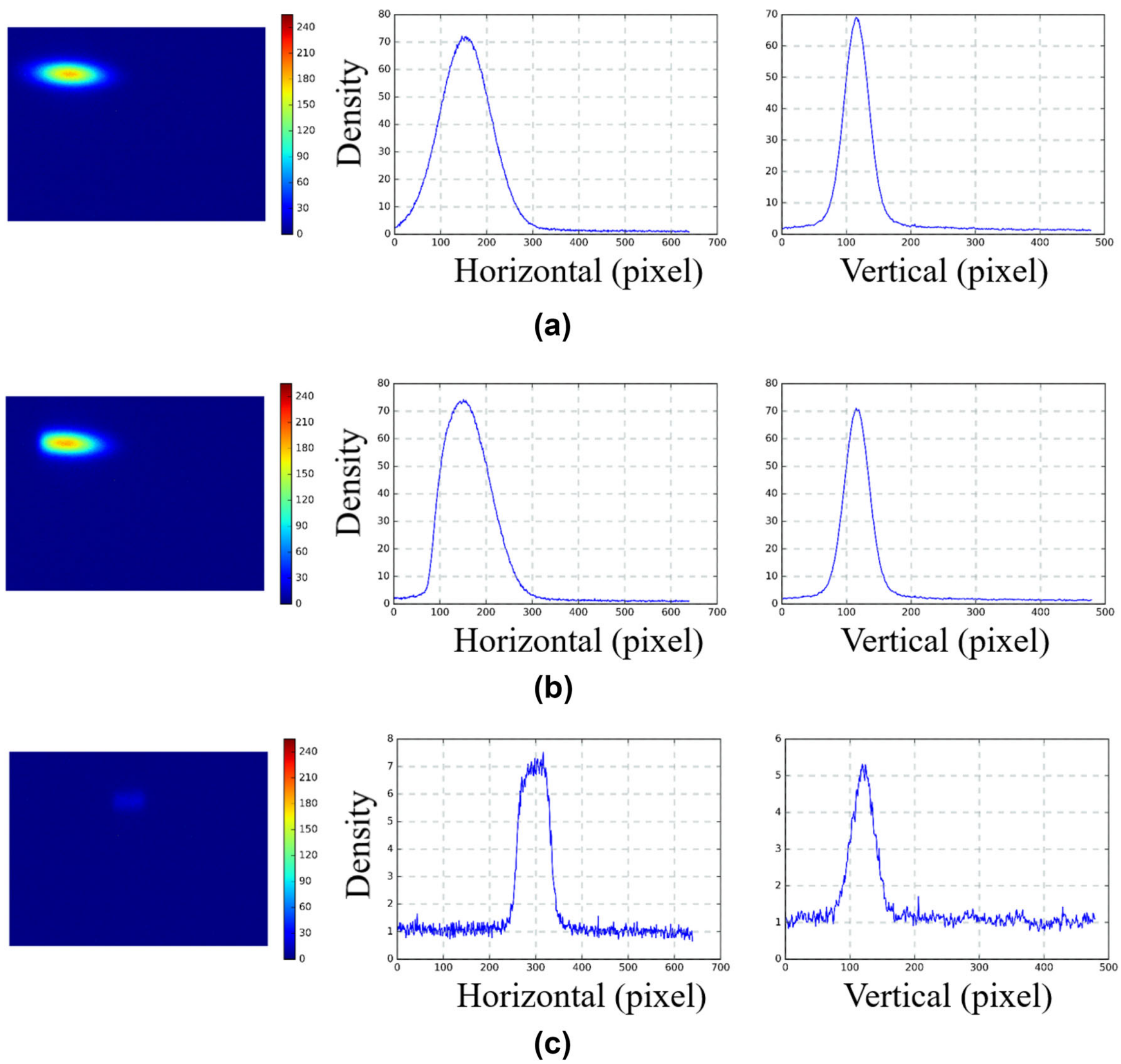

Fig. 6 (Color online) Images and profiles as the crystal was moved into the beam. **a** Image and profile before the crystal cuts the X-ray. **b** Only the edge of the crystal cuts the X-ray. **c** X-rays reflected from the crystal

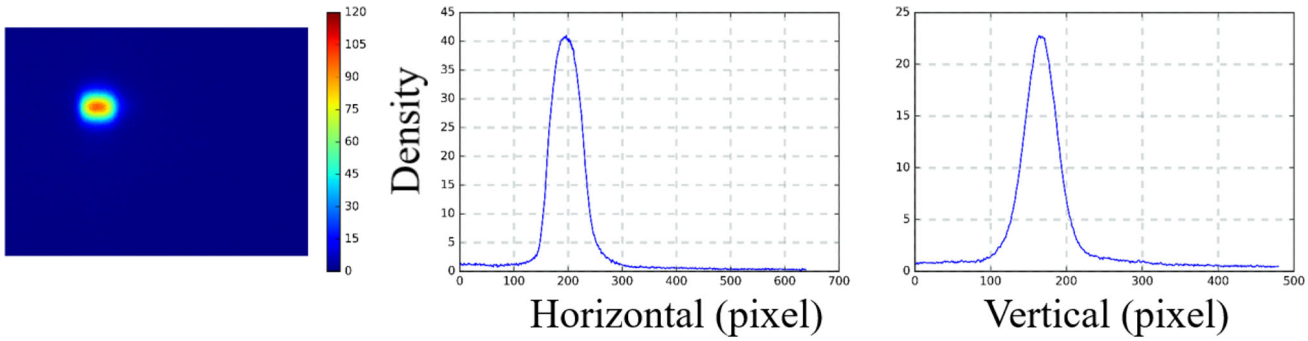

Fig. 7 (Color online) Image without Cu filter

obtained from experiments. The intensity of the images obtained from the CCD camera can be used to reflect the intensity of the X-rays. In this work, the sum of the intensities of the images is used to characterize the intensity of the X-rays. By adjusting the angle of the crystal, X-rays with different wavelengths or energies can be obtained, and the spectrum of the extracted X-ray photon beam can be scanned out. In order to obtain the wavelength value corresponding to each intensity, the theoretical spectrogram needs to be used as a reference. The theoretical spectrum can be calculated using the X-ray Oriented Programs (XOP) [14].

Figure 8 shows the theoretical photon beam spectra calculated by XOP after passing through a 1 mm Al window and a 2 mm Cu filter. These curves can be used to fit the spectrum obtained from the experiment, and it is then possible to obtain the wavelength. Figure 9 shows the integrated intensity of images at each angle, where the glancing angle of the X-ray was changed from large to small in 0.30 deg increments.

By fitting the experimental data in Fig. 9, the wavelength can be extracted. The energy of the peak intensity

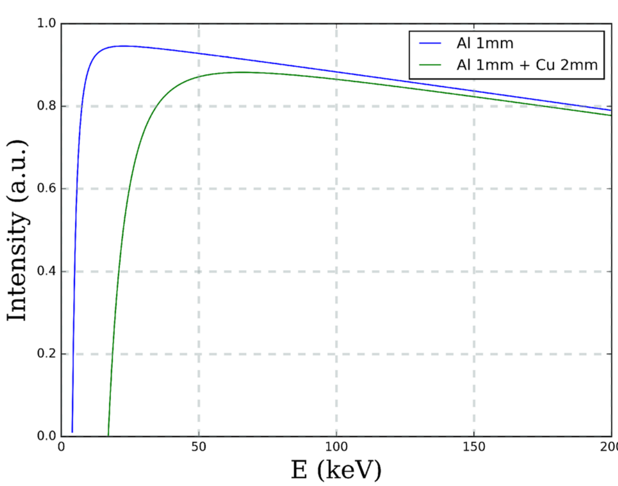

Fig. 8 (Color online) Extracted X-ray spectrum in the X-ray diagnostic beam line at SSRF

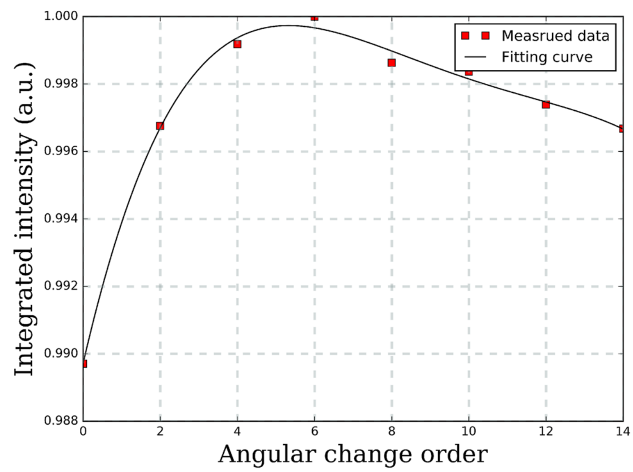

Fig. 9 (Color online) Integrated intensity of images at each angle

obtained at this experiment is 28.7 keV, the wavelength is 0.043 nm, and the glancing angle is 3.92 deg. According to Eq. 3, the PSF of the diffraction pattern is 5.5 µm, while the calculated diffraction contribution of the white X-ray is 6.0 µm [7].

3.3 Beam-based calibration

The idea of the novel beam-based calibration technique requires adjusting the angle of the crystal and observing the image at the CCD camera. The PSF is then derived from these measurements.

Eq. 2 can be rewritten as follows:

$$\sigma_{\mathrm{img}}^2 - (C_{\mathrm{mag}}\sigma_{\mathrm{beam}})^2 = \sigma_{\mathrm{diff}}^2 + (\sigma_{\mathrm{aper}}^2 + \sigma_{\mathrm{scr}}^2). \tag{5}$$

The beam size σ_{beam} and the PSFs other than the diffraction contribution $(\sigma_{\mathrm{aper}}^2 + \sigma_{\mathrm{scr}}^2)$ are assumed to be constant. Using the diffraction width of PSFs, the size of the image, and the theoretical beam size, the complete PSF of the pinhole system can be derived.

The theoretical beam size can be described as follows [15]:

$$S^2 = \beta\epsilon + (\eta\sigma_\epsilon)^2, \tag{6}$$

where S is the beam size, β and η are the betatron and dispersion functions, respectively, and ϵ and σ_ϵ are the emittance and the relative energy spread of the electron beam, respectively. In this case, β is 12.65 m, σ_ϵ is 0.99×10^{-3}, η is 0.0, and ϵ is 32.3 pm-rad in the vertical plane. According to Eq. (6), the beam size in the vertical plane is 20.2 µm. The diffraction width can be calculated with the wavelength obtained from the previous subsection. We assume the beam size of 20.2 µm is constant.

Grazing angles and values of ${\sigma_{\text{diff}}}^2$, ${\sigma_{\text{img}}}^2$, and $\sigma^2_{\text{img}} - (C_{\text{mag}}\sigma^2_{\text{beam}})$ are shown in Table 1.

Table 1 shows the experiment data. According to Eq. 5, $(\sigma^2_{\text{aper}} + \sigma^2_{\text{scr}})$ is the only unknown variable. This parameter is determined using the measured image sizes and σ_{diff}. From the data shown in Table 1, the data conform to the trend represented by the formula, it is expected that the total PSF can be obtained. This is a multi-equation process of finding approximate solutions, which is more accurate than using a single equation. At the same time, this can effectively reduce the random error.

The combined value of the geometric and imaging system widths of the pinhole PSFs is determined to be 37.7 µm, and the calibrated complete PSF of the pinhole camera is 38.1 µm at a grazing angle of 3.92°.

3.4 Results and Discussion

According to the theoretical study of pinhole PSFs presented in Sect. 2, the calculated PSF is 18.4 µm, while the imaging system width is estimated to 10 µm. This calculated PSF is much smaller than the calibrated PSF. One possible reason is that Eq. 4 is not completely suitable for calculating the geometric width, which is based on the assumption of a Gaussian PSF. According to this consideration, simulations have been performed to calculate the PSF.

SRW [16] is a wave optics simulation code that can take the actual wave front of the light emitted by a filament-like source in the bending magnet, propagate it through the pinhole, and project it onto the scintillator. In this work, SRW code was used to calculate the theoretical PSF on the scintillator. In the simulation process, the vertical beam size was set to 20.2 µm, the optical path is shown in Fig. 5, and the photon energy was set to 28.7 keV. The image size obtained at the scintillator is 45.07 µm. In other words, the PSF on the scintillator is 33.35 µm.

Compared with the value obtained from simulation, the calibrated PSF is larger, and there are two possible reasons. The first is that the thickness of the pinhole is also an important factor. However, the thickness of the pinhole was not taken into account in the simulation. The second is that the imaging system width of pinhole PSFs was not contained in the simulation results.

According to the comparison between the theoretical values and the calibrated PSF, the calibrated PSF was larger but more comprehensive. In summary, the new experimental method can derive the PSF of the X-ray pinhole camera. Combined with the X-ray quasi-monochromator, the PSF calibration can be implemented during user operation without any particular beam conditions. With this method, the resolution of the pinhole camera will be higher and the PSF calibration become more convenient.

Table 1 The expected beam sizes and the corresponding Gaussian image sizes obtained for various grazing incidence angles

Angle deg	σ^2_{diff} (µm^2)	σ^2_{img} (µm^2)	$\sigma^2_{\text{img}} - (C_{\text{mag}}\sigma_{\text{beam}})^2$ (µm^2)
4.82	45.2	2394.2	1475.2
4.52	39.7	2395.8	1476.8
4.22	34.7	2375.0	1456.0
3.92	29.9	2388.3	1469.3
3.62	25.5	2365.3	1446.3
3.32	21.5	2340.3	1421.3
3.02	17.7	2344.6	1425.6
2.72	14.4	2339.3	1420.3

4 Application

For a user facility such as SSRF, it is crucial to maintain the stability of the beam in the storage ring. A transverse feedback system has been developed to suppress beam instability in the storage ring. Beam size measurement can be used to characterize the performance of the transverse feedback system [17]. An experiment has been conducted to verify the performance of the new X-ray pinhole camera, where the gain of the feedback system is adjusted and the resulting beam size is measured. The results are shown in Fig. 10.

While the gain of the transverse feedback system is under 100 dB, the system is in the low-feedback process. If the gain changes from 90 to 96 dB, the observed beam size changes from 50.8 to 20.9 µm. When the gain is between 96 and 288 dB, the system is working in the regular mode, and the observed beam size remained stable. While the gain is more than 288 dB, the system is in the over-feedback process, the observed beam size changes increases from 21.1 µm.

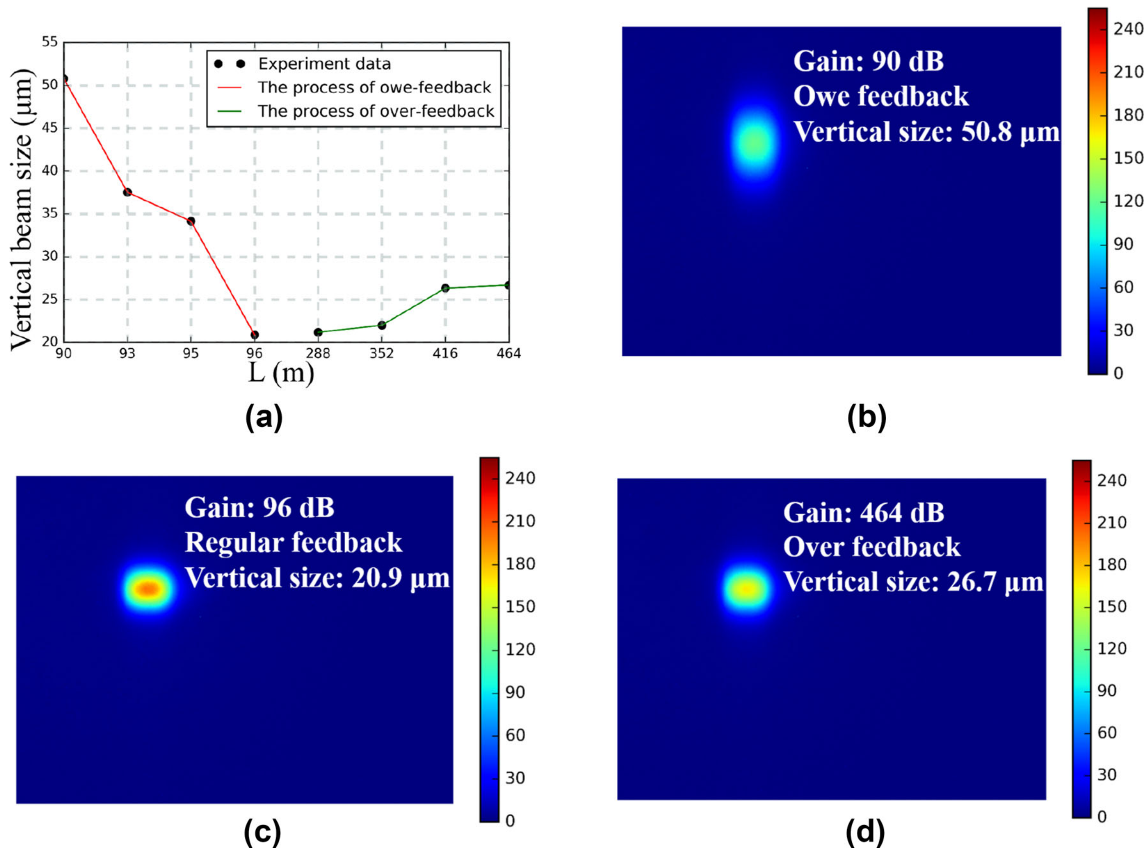

Fig. 10 (Color online) Adjusting the gain of the transverse feedback system. **a** The process of adjusting the gain. **b** beam imaging with underfeed conditions, **c** beam imaging with regular conditions. **d** beam imaging with overfeed conditions

5 Conclusion

An X-ray quasi-monochromator has been installed at SSRF. A novel beam-based experimental method was introduced to calibrate the PSF of the X-ray pinhole camera at SSRF using this monochromator. By adjusting the angle of the crystal monochromator to select a defined X-ray wavelength and measure the image size, the PSF can be accurately resolved. The spectrum of the extracted X-ray can be obtained from the experiment. The new X-ray pinhole camera can also be used to observe the effects of the transverse feedback system.

Acknowledgements The authors would like to thank the operation and physics group at SSRF for their assistance during the experiments.

References

1. A.H. Lumpkin, B.X. Yang, C.Y. Yao et al., X-ray Imaging of the APS storage ring beam stability effects: From the Alaskan earthquake to undulator field changes, in *PAC2003*, pp. 2423–2425 (2003)
2. M.J. Boland, M. Spencer, vertical beam profile measurement and analysis with an X-ray Pinhole, in *EPAC08*, pp. 1059–1061 (2008)
3. J.C. Bergstrom, J.M. Vog, The X-ray diagnostic beamline at the Canadian Light Source. Nucl. Instrum. Methods A **578**(2–3), 441–457 (2008). https://doi.org/10.1016/j.nima.2008.01.080
4. C.A. Thomas, G. Rehm, Fast pinhole camera for optimization of top up injection, in *BIW08*, pp. 279–281 (2008a)
5. G.Q. Huang, J. Chen, Z.C. Chen et al., X-ray pinhole camera control system design for SSRF storage ring. Nucl. Tech. **34**, 641–645 (2011). (in Chinese)
6. G.Q. Huang, J. Chen, Z.C. Chen et al., X-ray pinhole camera system design for SSRF storage ring. Nucl. Tech. **33**, 806–809 (2010). (in Chinese)
7. Y.B. Leng, G.Q. Huang, M.Z. Zhang et al., The beam-based calibration of an X-ray pinhole camera at SSRF. Chin. Phys. C **36**, 80 (2012). https://doi.org/10.1088/1674-1137/36/1/014
8. F. Ewald, P. Elleaume, L. Farvacque et al., Vertical emittance measurement at the ESRF, in *MOPD61, DIPAC*, p. 11 (2011)
9. Gero Kube et al., PETRA III diagnostics beamline for emittance measurements, in *Proceedings of 1st International Particle Accelerator Conference: IPAC*. Vol. 10. (2010)
10. https://www.britannica.com/science/spectroscopy/Energy-states-of-real-diatomic-molecules#ref80642
11. http://www.global-optosigma.com/en_jp/
12. P. Elleaume, C. Fortgang, C. Penel et al., J.Synchrotron Rad 2, pp. 209–214 (1995)
13. Z.C. Chen, Y.B. Leng, J. Chen et al., MOPME053: Point spread function study of X-ray pinhole camera in SSRF, in *Proceeding of IPAC*. Shanghai, China, pp. 12–17 (2013)

14. Manuel Sánchez del Río, Roger J. Dejus, XOP v2.4: recent developments of the x-ray optics software toolkit, in*Proceedings of SPIE 8141, Advances in Computational Methods for X-Ray Optics II* (2011). https://doi.org/10.1117/12.893911
15. C.A. Thomas, G. Rehm, TUPC086: Pinhole camera resolution and emittance measurement, in *Proceeding of EPAC*, Genoa, Italy, 23–27 (2008)
16. O. Chubar, P. Elleaume, Accurate and efficient computation of synchrotron radiation in the near field region, in *EPAC98, THP01G*, pp. 1177–1179
17. J. Chen, Z.C. Chen, Y.B. Leng et al., MOPB70: The synchrotron radiation diagnostic line At SSRF, in *Proceeding of IBIC, Tsukuba*, Japan, pp. 1–4 (2012)